

DIAGNOSTIC DEVELOPMENTS AT CERN'S SRF TESTING FACILITY

A. Macpherson*, K. Hernandez Chahin, S.Aull, A. Benoit, P. Fernández López, C. Jarrige, P. Maesen, K.-M. Schirm, R. Torres-Sanchez, R. Valera Teruel, CERN, Geneva, Switzerland
 T. Junginger, TRIUMF, Vancouver, Canada

Abstract

As part of CERN's re-establishment of an SRF cold testing facility for bulk niobium cavities, diagnostic instrumentation and testing procedures on our vertical cryostat have been upgraded, with particular attention given to quench location, ambient magnetic field control, thermometry and thermal cycling techniques. In addition, preparation and measurement procedures have been addressed, allowing for improved measurement of cavity properties and detailed study of transient effects during the course of cavity testing.

INTRODUCTION

As part of CERN's R&D programme on bulk Niobium cavities [1], considerable effort has been invested in the refurbishment of the vertical cryostat test stand at our SRF test facility [2]. Included in this refurbishment has been an upgrading of measurement hardware and the addition of a full suite of diagnostic tools. For the measurement infrastructure, the setup is as shown in Fig. 1, with the test stand operating at 2K in CW mode with a fixed input coupler, and a maximum input power of 260W.

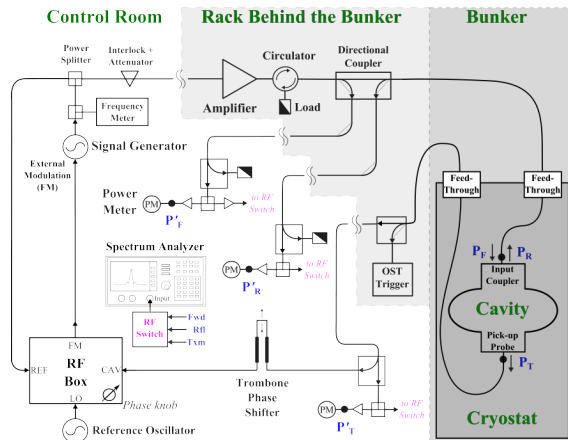


Figure 1: Schematic of the vertical test cryostat setup.

MEASUREMENT TEST STAND

As part of the refurbishment, the test stand software has been completely re-written in LabView, and now uses an underlying queue-based manager handler structure. This has resulted in significant improvement in data taking capabilities, with data acquisition rates of 3 Hz for Q_0 vs E_{acc} scans. This permits detailed semi-automated power scans with small incremental input power steps (typically 0.05 dBm), which in turn allows us to clearly scan and identify

multipacting sub-structure of the cavity, as can be seen in Fig. 2. Data sets for a typical detailed scan contains about six thousand data points, where each data point is a data object containing both measurement and environmental data. Also seen in Fig. 2 is the transient behaviour of the cavity on increment of the input power, which can be used to estimate the cavity filling time, and hence give a cross-check of the test stand calibration.

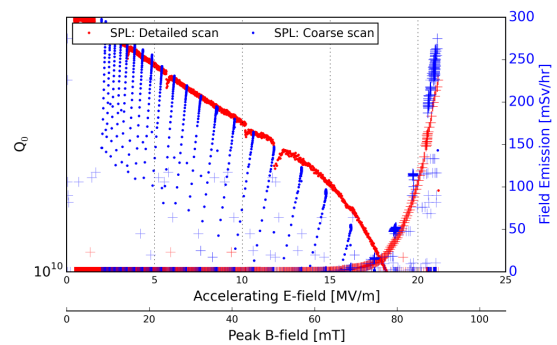


Figure 2: A detailed Q_0 vs E_{acc} scan for a cavity. The scan with a coarse incremental power step is in blue, while the red points show the same cavity scanned with 0.05 dBm increments. The detailed scan reveals a sub-structure most likely small multipacting barriers. Radiation data from the field emission is shown as a "+".

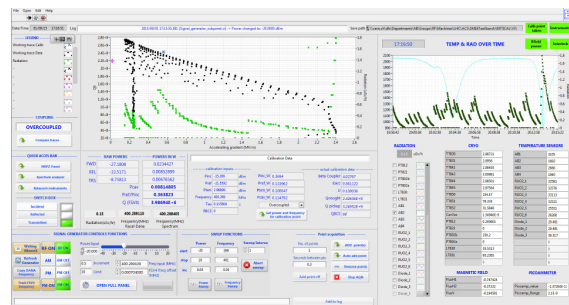


Figure 3: Front panel display of the LabView software framework used for the SRF test stand. Scan results are on the left and environmental monitoring data on the right.

For the cavity environment monitoring, on-line diagnostics have been installed and validated. These include contact resistors used as cavity temperature sensors, fluxgate magnetic field probes for ambient field measurements, and standard monitoring of field-emission induced radiation, cavity vacuum, and the full monitoring of the cryo process and operation. All monitoring data is available at the top level of the data taking application for real-time display (see Fig. 3), and is time stamped and stored. Due to the large increase in measurement and environmental data, a hierarchical data storage

* alick.macpherson@cern.ch

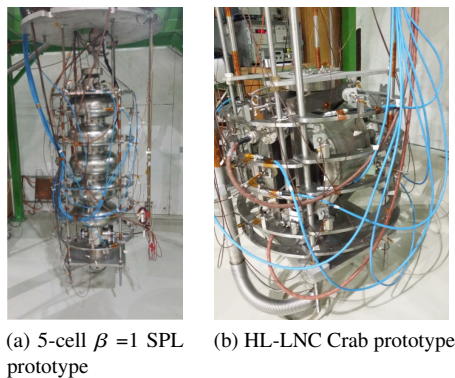


Figure 4: The cryostat insert prior to installation in the cryostat, with cavity and diagnostics installed.

structure has been adopted, including metadata tagging, with the data storage done in the HDF5 package [3]. HDF5 offers easy hierarchical data browsing with cross-platform support. For off-line processing of the measurement data a full suite of analysis routines has been written in the Python language, and is maintained in an SVN repository to ensure integrity of the analysis routines.

DIAGNOSTICS SETUP

Implicit in the measurement procedure is a need for robust diagnostics, in order to set the experimental conditions and to diagnose cavity performance issues. The present test stand diagnostics includes 18 channels of temperature monitoring using contact temperature resistors (CERNOX, RuO₂, and Allen Bradley), cavity and helium bath pressure gauges, 3 single axis magnetic fluxgate probes for ambient magnetic field measurement, and a 30 sensor array for quench localisation. Installation of all instrumentation on the cryostat insert is done with careful attention to cable shielding and grounding, with a well-defined star point grounding established at the readout rack immediately behind the cryostats shielding. Examples of the fully instrumented insert for a 5-cell $\beta = 1$ elliptical cavity and a compact crab cavity can be seen in Fig. 4.

For the operational procedure, the most crucial aspects that had to be addressed were the issue of ambient magnetic field around the cavity and the effect of cool down on the RF performance. As the vertical test cryostat has no static magnetic shielding, three compensation coils are used to provide the required level of screening. Once the cavity insert is installed in the cryostat, a feedback loop on the coils is used to set the required ambient magnetic level. Input into the feedback loop is from the fluxgate probes, and the feedback loop allows magnetic field along any axis to be set within the range 5 nT to 60 μ T. For testing, the magnitude of the magnetic field is typically set below 30 nT.

Cool down is done with the thermal shield pre-cooled, so that the cavity cools rapidly from room temperature to 15 K. This is done as rapidly as possible, with typical cool down rates of order 15 K/min, to avoid excessive formation

of niobium hydrides and the onset of Q-disease in the 100 K to 50 K. No stop at 100 K is made to check for Q-disease.

With such a rapid cool down, large spatial thermal gradients on the cavity (in excess of 200 K) are observed, which create the expected large thermal-electric currents over the cavity length, as can be seen in Fig. 5a, via the variations in the ambient magnetic field. For controlling the thermal and mechanical conditions when the cavity goes through the superconducting transition at $T_c \approx 9.2$ K, effort has been made with the cryogenics operation team to establish full control of the spatial thermal gradient and the cool down rate, so that the transition through T_c is user configurable. Figure 5 b and c show the range of cool down options (in addition to fast cool down with a large spatial temperature along the cavity). Complete expulsion of the trapped flux is not yet achieved due to some of the insert support infrastructure (cavity pumping line) that provide current paths for thermal electric currents to circulate. Modifications to ensure electrical isolation of the cavity are presently in preparation. Our typical cool down cycle is a rapid cool down to 15 K, then pausing the cooling till the cavity is thermalised, before compensating the ambient magnetic field. The cavity is then cooled through T_c with an ambient spatial thermal gradient of 5 K to 10 K. Cool down speeds of 1 K/min and a spatial thermal gradient of about 5K has been found to give similar RF performance as a fast cool down directly to 4 K [1], but as shown in Fig. 5, spatial temperature gradients over the cavity length as low as 0.5 K can be achieved.

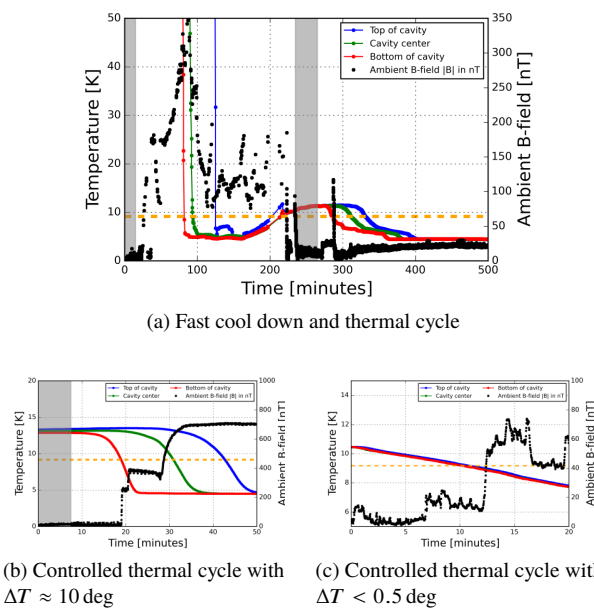


Figure 5: Cool down of the cavity and the observed thermal electric currents, as seen by the effect on the ambient magnetic field. Control of the spatial thermal gradient at transition ranges from uncontrolled (a), to a well defined (b), and less than 0.5 K (c). The grey bands show when the compensation coils feedback loop was active to suppress the ambient magnetic field to < 30 nT.

PERFORMANCE DIAGNOSTICS

In terms of diagnostics during cavity powering, temperature monitoring and quench localisation form the basis of our diagnostics platform. For temperature monitoring, an array of 18 temperature sensors is used, with a mix of sensor types (CERNOX, Allen Bradley 120 Ω resistors and surface mount Ruthenium Oxide resistors). Thermal contact to the cavity surface is by direct contact, using either aluminium adhesive tape or a spring loaded holder, with thermal grease applied if a flat contact surface is not available. In-situ calibration is done for each cold test, with the superconducting transition at T_c and the superfluid transition used as absolute reference points for calibration. Readout is by a standard programmable logic controller based readout system, that sends 10 μ A measurement pulses. This system provides temperature monitoring rather than temperature mapping capabilities, but as seen from Fig. 6, the online system allows us to see thermal loading of a cavity during a power scan. Figure 6 illustrates the warming of the high E-field region in an RF Dipole HL-LHC crab cavity prototype.

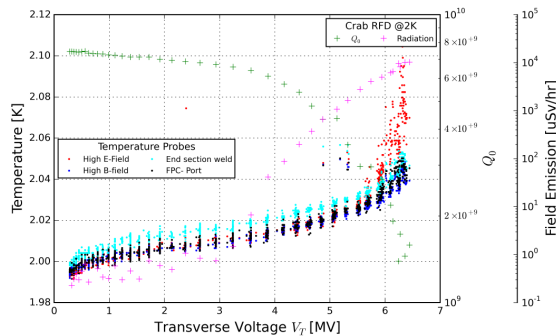


Figure 6: Thermal monitoring of an HL-LHC crab cavity prototype, with heating observed in the high E-field region when reaching high transverse voltage.

For quench localisation, Oscillating Superleak Transducers (OSTs) [4] are used, with a sensor array of 30 OSTs deployed around the cavity. When quenches occur, the OSTs are used to detect the second sound waves produced by the quench, and with three or more signals a trilateration can be done to locate the quench spot. For this system to operate effectively at 2 K, particular attention was given to the grounding scheme of these sensors. To ensure an acceptable signal to noise ratio, electrical isolation of the sensor from the insert support structure and shielding of cabling back to the grounding star point has proven to be essential. Figure 7 shows a typical OST signal from a mid-field quench of an SPL cavity. For the trigger signal used to time stamp the quench, the power signal from the cavity pickup has been observed to be out of synch with the OST signals; for a multi-cell cavity, particularly for mid-field magnetic field induced quenches, the transmitted power signal from the pickup was not necessarily synchronised with the quench, and was not suitable as a reliable trigger. Here, the suspicion is that the cavity field collapse, as measured by the pickup, is dependent on the strength and the relative location of the

ISBN 978-3-95450-178-6

780

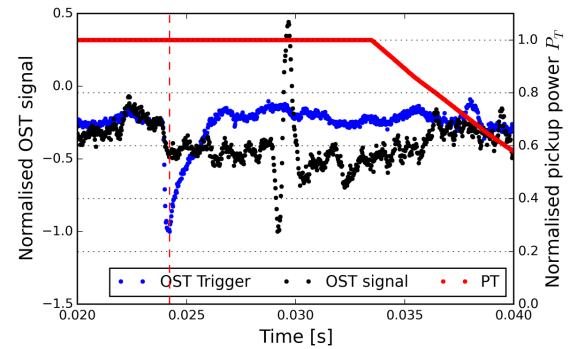


Figure 7: OST trigger (1st sound), a typical OST data signal (2nd sound) and transmitted power from a mid-field quench of the SPL1 prototype just after the turn-on of field emission.

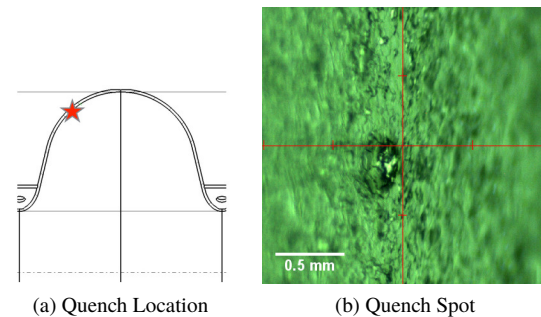


Figure 8: Identified quench spot found by optical inspection.

quench spot. For small to moderate quenches, variations in the onset of cavity field collapse can occur.

However, we observed that for triggering of the quench, a subset of the OST sensors with taut superleak film on the sensor face were sensitive to both the second sound signal, and to a sharp signal pulse occurring well before the second sound signal. This signal was reproducibly seen on a set of OSTs, and its relative time position suggest it is associated with the first sound density wave from the quench. Comparison of the OST signal, this trigger signal, and the transmitted power signal from the pick-up antenna are shown in Fig.7.

Using signals from this OST array, an example of the second sound trilateration for a mid-field quench of a 5-cell bulk Niobium cavity at 2 K is shown in Fig. 8. The difference between the predicted quench spot and the location, as identified by optical inspection of the surface, was $\Delta\theta = 1.9^\circ$ and $\Delta z = 9.5\text{mm}$, and the average propagation velocity associated with the second sound was estimated at 30.5 m/s. This velocity is a parameter of the trilateration process, and is sometimes interpreted as the second sound velocity. The value obtained from the trilateration is higher than the typical second sound velocity at this temperature, but it is in line with similar values obtained from quench location trilaterations on other cavities [5]. Further, the fact that this defect occurred in a high magnetic field region of the cavity where the surrounding surface area was otherwise unremarkable lends to the veracity of the quench spot identification.

SRF Technology - Cavity

E08-Cavity Testing Diagnostics

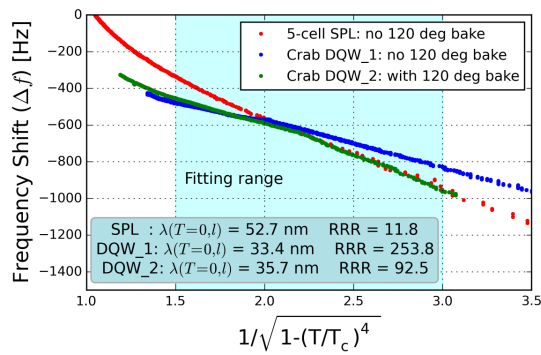


Figure 9: Frequency shift as a function of temperature, to give the penetration depth, mean free path and RRR.

PROCEDURAL IMPROVEMENTS

As part of the cavity validation, the measurement of penetration depth was seen as a key measurement, but due to infrastructure limitations, one that we were not able to do. For this measurement, the change in penetration depth is proportional to resonant frequency shift as the cavity is isothermally warmed toward the superconducting transition at T_c . From the frequency shift, the penetration depth, mean free path and residual resistance ratio (RRR) can be extracted [6]. However, for our cryostat the diagnostic issues were reliable frequency tracking as $T \rightarrow T_c$ and stable cryostat pressure conditions during the isothermal heating.

With the upgrade of the measurement hardware, and careful calibration of measurement offsets, frequency tracking at the sub-hertz level has been achieved. For stable measurement conditions, it was necessary to stabilise the cryostat pressure over the duration of the measurement. Yet, with a 3400 litre vertical cryostat, this was extremely difficult, as the large volume meant the measurement was overshadowed by frequency fluctuations from the cryogenics system. Any attempt to do this measurement with the cryostat at or near atmospheric pressure was unsuccessful, due to pressure fluctuations inherent in the cryogenic system.

To accurately measure the frequency shift associated with the penetration depth, we changed the operational procedure such that the liquid helium was evaporated until the cavity was completely out of the liquid, and only a small liquid level remained at the bottom of the cryostat. The cryostat was then pumped down to a pressure of 28 mbar and was maintained at this level to within 0.2 mbar, due to the capacity of the pumping line. Isothermal warmup was then done by balancing the heating power of the evaporator installed beneath the cavity against the vapour cooling from the remaining liquid, where the heat transfer from the evaporator to the liquid helium was via copper braid grounding straps hanging from the evaporator. In this way, the cavity could be warmed from 4 K to 10 K over a 4 hour period, with less than 0.5 K spatial temperature gradient. During this time, resonant frequency was continuously tracked and recorded. The measurements from three such warm-ups is shown in Fig. 9. The resulting RRR values for the HL-LHC Crab



Figure 10: Image of the corroded HPR nozzle.

prototype before and after chemistry seem reasonable, while the RRR value for the SPL prototype cavity is rather low, given that it did not have a 120 °C prior to testing. However, this suggested a low RRR layer sitting on the high RRR bulk, due to possible surface contamination during the HPR step.

HIGH PRESSURE RINSING

As seen from the RRR measurements of the SPL prototype, there was cause to believe that we had some level of RF surface contamination, and indeed, inspection showed that a component in the high pressure rinse system was exhibiting signs of corrosion. As can be seen from Fig. 10 the HPR nozzle head (made from stainless steel 400, and rated for 1500 psi operation), was not suitable for 100 bar pressure with ultra-pure water, and progressively corroded. The nozzle head has since been replaced, and additional particle counter instrumentation added to the HPR system to avoid a repetition of this problem.

The issue with the corroded nozzle has been one of a number of commissioning issues experienced with HPR cleaning and assembly in our new SRF ISO4 cleanroom [2]. The HPR system is a 100 bar high pressure rinse system from SPEC [7] with a di-jet nozzle that moves vertically while the cavity rotates. As part of the process of gaining operational experience with this system, recent RF tests [1] indicate that the HPR and clean room process is not yet optimised, and a full HPR and assembly procedure has yet to be established. In particular for elliptical cavities tested, field emission has been an issue, while for compact crab cavities the RF results indicate surface contamination due to insufficient cleaning of the entire cavity surface and/or possible surface deterioration due to the drying after the HPR.

At present, we operate the HPR system with a nozzle that produces a flat spray water jet with a spray angle of 25°, and our standard HPR consists of a 6-cycle rinse, where the vertical nozzle speed is 0.5 mm/s and the cavity rotation is 3 RPM. With these parameters an overlapping water jet coverage is achieved, but it is not ideal, and the vertical nozzle speed is too high compared to settings used in other SRF labs. Firmware changes have been implemented in order to reduce the vertical nozzle speed to 0.1 mm/s, and the HPR efficiency is now being re-evaluated.

In order to optimise the cleaning efficiency of the HPR, a transparent 2-cell elliptical cavity based on the 704 MHz SPL cavity design has been constructed out of plexiglass (see Fig.11a), and instrumented with transient pressure data loggers. Ongoing tests have shown that the expected pressure on the cavity surface is markedly lower than expected, due primarily to the nozzle head design. Measured pressures at a approximately 6 cm distance range between 18 and 26 bar. A full optimisation of the HPR has not yet been completed, as a compromise between water-jet spray angle and vertical nozzle speed has yet to be found. However, validation of the HPR settings is now done using a DESY 1.3 GHz bulk niobium cavity (see Fig.11b) as a calibrated test cavity, with the effectiveness of the cleaning characterised by the achieved gradient and field emission onset gradient.

With the standard HPR as listed above, a residual resistance of 10 n Ω to 13 n Ω has been reached for this test cavity, and a typical field emission onset around 17 MV/m. This level of cleanliness still needs improvement for production operation.



(a) HPR test of transparent cavity model

(b) 1.3GHz test cavity used for RF tests of HPR effectiveness

Figure 11: HPR optimisation is done with two test structures: (a) A transparent cavity used for HPR optimisation tests, and (b) a 1.3 GHz elliptical cavity used to verify RF performance after different HPR recipes.

CONCLUSION

As part of the refurbishment of CERN's SRF vertical test stand for bulk niobium, significant effort has been invested in the upgrade and implementation of diagnostic infrastructure, with clear gains in measurement performance and data quality. For a system with simple phase lock loop tracking of the cavity resonance frequency, a restructured queue based data acquisition framework has allowed for detailed measurement as well as tracking of transient cavity behaviour. This, coupled with the implementation of a full set of environmental diagnostics now provides a fully operational vertical test cryostat. Progress has been made with both quench spot localisation via second sound trilateration, and penetration depth measurements, due to changes in operational procedure and experience with the test stand operation. Additionally, the HPR step of the cavity surface preparation is being progressively improved, with performance tests of the

HPR done using a transparent cavity mockup, and verified with a 1.3GHz test cavity.

REFERENCES

- [1] A Macpherson, K. Hernandez Chahin, C. Jarrige, P. Maesen, F. Pillon, K.-M. Schirm, R. Torres-Sanchez, and N. Valverde Alonso. CERN's Bulk Niobium High Gradient SRF Programme: Developments and Recent Cold Test Results. In *These proceedings*, SRF2015, Whistler, Canada, MOPB074.
- [2] J. Chambrillon, M. Therasse, O. Brunner, P. Maesen, O. Pirotte, B. Vullierme, and W. Weingarten. CERN SRF assembling and test facilities. *Proc. SRF11, Chicago, USA, 2011*, TUPO058.
- [3] HDF Group - HDF5, 2015.
- [4] Z. A. Conway, D. L. Hartill, H. S. Padamsee, and E. N. Smith. Oscillating superleak transducers for quench detection in superconducting ILC cavities cooled with He-II. *Proceedings of LINAC08, Victoria, BC, Canada THP036*, 2008.
- [5] T. Junginger, P. Horn, T. Koettig, B. Macpherson, B. Peters, and K. Liao. High Flux Three Dimensional Heat Transport in Superfluid Helium and Its Application to a Trilateration Algorithm for Quench Localisation With OSTs. In *These proceedings*, SRF2015, Whistler, Canada, MOPB049.
- [6] Gianluigi Ciovati. Effect of low-temperature baking on the radio-frequency properties of niobium superconducting cavities for particle accelerators. *Journal of Applied Physics*, 96(3):1591–1600, 2004.
- [7] SPEC - Semiconductor Process Equipment Corporation | Wet Bench Manufacturer | Wet Process, 2015.